

See discussions, stats, and author profiles for this publication at: <https://www.researchgate.net/publication/221809675>

Receptor-Ligand Interaction-Based Virtual Screening for Novel Eg5/Kinesin Spindle Protein Inhibitors

ARTICLE in JOURNAL OF MEDICINAL CHEMISTRY · MARCH 2012

Impact Factor: 5.45 · DOI: 10.1021/jm201290v · Source: PubMed

CITATIONS

15

READS

45

4 AUTHORS, INCLUDING:



[Shanthi Nagarajan](#)

Oregon Health and Science University

13 PUBLICATIONS 121 CITATIONS

[SEE PROFILE](#)



[Dimitros Skoufias](#)

Institut de Biologie Structurale (IBS)

42 PUBLICATIONS 1,888 CITATIONS

[SEE PROFILE](#)



[Ae Nim Pae](#)

Korea Institute of Science and Technology

179 PUBLICATIONS 1,491 CITATIONS

[SEE PROFILE](#)

Receptor–Ligand Interaction-Based Virtual Screening for Novel Eg5/Kinesin Spindle Protein Inhibitors

Shanthi Nagarajan,^{†,‡} Dimitrios A. Skoufias,[§] Frank Kozielski,[⊥] and Ae Nim Pae*,^{†,‡}

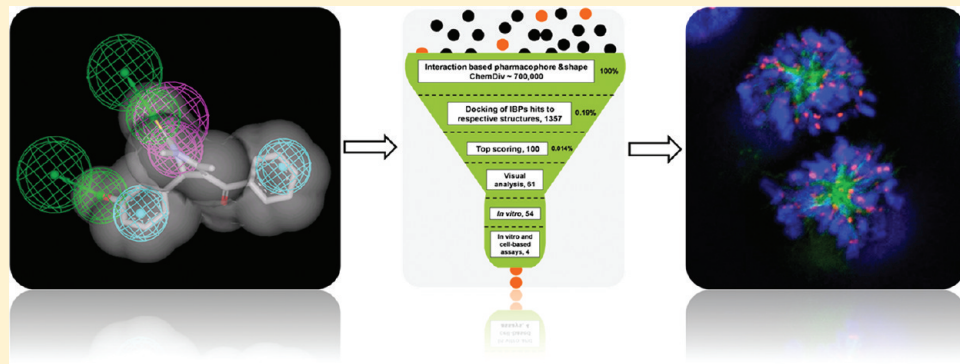
[†]Neuro-Medicine Center, Life Sciences Division, Korea Institute of Science and Technology, PO Box 131, Cheongryang, Seoul 130-650, Republic of Korea

[‡]School of Science, Korea University of Science and Technology, 52 Eoeun dongYuseong-gu, Daejeon 305-333, Republic of Korea

[§]Institute for Structural Biology (CEA-CNRS-UJF), 41 rue Jules Horowitz, 38027 Grenoble Cedex 1, France,

[⊥]The Beatson Institute for Cancer Research, Garscube Estate, Switchback Road, Bearsden, Glasgow, G61 1BD, Scotland, U.K.

 Supporting Information



ABSTRACT: Eg5/KSP is a promising mitotic spindle target for drug discovery in cancer chemotherapy and the development of agents against fungal diseases. A range of Eg5 targeting compounds identified by in vitro or cell-based screening is currently in development. We employed structure-based virtual screening of a database of 700 000 compounds to identify three novel Eg5 inhibitors bearing quinazoline (**24**) or thioxoimidazolidine (**30** and **37**) scaffolds. The new compounds inhibit Eg5 ATPase activity, show growth inhibition in proliferation assays, and induce monostral spindles in cells, the characteristic phenotype for Eg5 inhibiting agents. This is the first successful reported procedure for the identification of Eg5 inhibitors via receptor–ligand interaction-based virtual screening.

INTRODUCTION

Kinesins are a large superfamily of motor proteins that participate in various biological phenomena including mitosis and intracellular transport of vesicles and organelles.¹ Kinesin spindle protein (KSP, also known as HsEg5) is a slow, plus end-directed motor of the kinesin-5 subfamily.^{2,3} Kinesin-5 exists as a homotetramer, where two kinesin-5 dimers bind together in an antiparallel manner to form a “dumbbell-shaped” molecule.⁴ Kinesin-5 cross-links microtubules (MTs) of opposite polarity and slides them apart.⁵ Consequently, kinesin-5 plays a critical role in bipolar spindle formation during mitosis, and inhibition of Eg5 function leads to cell cycle arrest at mitosis with the formation of monostral spindles and, ultimately, to cell death under certain conditions.³ Mitotic arrest provokes apoptosis mainly through the intrinsic apoptotic pathway.⁶

The clinical relevance of blocking tubulin function in anti-cancer therapy has been demonstrated by, for example, taxol. Taxol is a well-characterized MT inhibitor approved for breast cancer treatment⁷ as well as ovarian, lung, bladder, prostate, melanoma, and esophageal cancers. Inhibition of tubulin can lead to cell division arrest and subsequent apoptosis of cancerous

cells.^{8,9} A number of other compounds interfering with tubulin dynamics have also been reported such as vinca alkaloids, colchicines, and synthetic agents. However, these compounds suffer from solubility problems, neurotoxicity, drug resistance, and disruption of cellular transport.^{10,11} Because these tubulin inhibitors have undesirable effects, it is necessary to investigate possible alternative targets, which may have a better safety profile.

One alternative target is Eg5. In humans, Eg5 is not involved in postmitotic processes, such as neuronal transport, and its inhibition is not expected to cause the peripheral neuropathy that is often associated with tubulin-targeting agents.¹² The important role of Eg5 in mitotic progression makes it a promising new target for drug discovery. Furthermore, it is most abundant in proliferating human tissues and is highly expressed in tumors of the breast, colon, lung, ovary, and uterus.³ Given the likelihood of an improved safety profile through targeting Eg5, it is desirable to identify and investigate small molecule inhibitors for this target. A number of Eg5 inhibitors have been reported,

Received: July 22, 2011

Published: February 6, 2012

namely ipinesib,¹³ MK-0731,¹⁴ ARRY-520,^{15–17} monastrol,¹⁸ S-trityl-L-cysteine,¹⁹ and several other small molecules.^{20–27} Ispinesib is a well understood Eg5 inhibitor currently in multiple phase II clinical trials. It has an acceptable safety profile with no indications of neurotoxicity^{13,28} and is 40 000 times more active against Eg5 compared to other kinesins.²⁹ As a result of these encouraging findings, we have undertaken a virtual screen to discover further Eg5 inhibitors.

In the modern drug discovery process, virtual screening (VS) offers an integrated approach that may lead to the identification of novel lead molecules.^{30,31} Virtual screening can be largely divided into two approaches, the first being a ligand-based virtual screening including the use of druglike filters, 2D similarity,³² 3D-shape,³³ pharmacophore,³⁴ field-screen,³⁵ QSAR,³⁶ and QSPR.³⁷ These methods can be used to filter down a large database into a few compounds. A second method is based on structure-based virtual screening. According to this method, a receptor binding site is used to screen small molecule libraries by means of docking.³⁸ Although a huge amount of structural data has been published for this target, no successful method for structure-based virtual screening has been reported yet. So far, Liu et al.³⁹ developed a four-feature pharmacophore model and Jiang et al.⁴⁰ docked various known Eg5 inhibitors and explained the importance of the minor binding pocket in increasing the binding affinity.

A number of research groups have produced successful results by combining ligand- and structure-based models in VS.^{41–43} To date, there is an increasing number of crystal structures of KSP in complex with different inhibitors available in the protein data bank (PDB).⁴⁴ In the present work, we have developed interaction-based pharmacophore models (IBPs) and applied them to filter the ChemDiv database with the hits being passed to an in silico docking procedure. We have used six Eg5 crystal structures in complex with diverse ligand structures for pharmacophore modeling and 16 structures to validate our docking protocol. The use of a number of pharmacophore models generated from various crystal structures could reflect successfully various inhibitor binding modes.⁴¹ Docking of several ligands into their respective crystal structures by FlexX, FlexX-Pharm, Surflex, LigandFit, GOLD, and GLIDE disclosed the best method that reproduces the bioactive conformation. In addition to the binding mode analysis, we have also conducted enrichment calculations to rationalize the suitable scoring function that ranks the active compounds at the top level of database sampling. From the various docking trials conducted, we identified that GOLD and GLIDE are optimal methods to regenerate the binding conformation close to the experimentally determined one, yielding high enrichment values. Therefore, we used both docking methods in VS following our pharmacophore search. Screening of the ChemDiv database containing 700 000 compounds yielded three hits, which inhibit Eg5 in vitro, in proliferation assays of two tumor cell lines (HT-29 and DU-145), and induce monoastral spindles, the typical phenotype observed when inhibiting Eg5. To the best of our knowledge, this is the first report on successful virtual screening for novel Eg5 inhibitors.

RESULTS AND DISCUSSION

Generation of Pharmacophore Models. We report how a set of IBP models is generated from experimentally determined Eg5–ligand structures. In total, six IBPs with diverse ligands and interactions were used to develop seven pharmacophore models (Figure 1). Because in the Eg5 mon-97 complex (2IEH) the OH group oxygen acts as an electron acceptor

and the hydrogen is a donor, two pharmacophore models were developed. All pharmacophore models are composed of at least five features, with the exception of 2UYM, exhibiting six features, five of which are hydrophobic (Table 1). Every IBP has at least two hydrophobic features, which facilitate the ligand binding in the predominantly hydrophobic pocket. Hydrogen bonds formed by protein–ligand complexes within 3.5 Å were converted into acceptor or donor features in the IBPs.

Protocol Development for Structure-Based Design.

Docking results of several ligands to their respective protein conformations are summarized in Table 2. A smaller root-mean-square deviation (RMSD) ensures the closeness of the predicted with the experimental pose. It is apparent that the RMSDs for GOLD, SurFlex, and GLIDE are better than those of other docking protocols. LigandFit, FlexX-Pharm, and FlexX have higher deviations from the bioactive conformation. Not surprisingly, the mean RMSD for FlexX is not in an acceptable range when compared to others. However, introducing pharmacophore constraints allows prediction of the conformation of the experimental pose. Enrichment calculations were conducted to rationalize the docking results (Table 3). Among the various docking protocols tested, GOLD outperformed the others with enrichments of 394 at 1% sampling. Following GOLD, FlexX-Pharm and Glide have enrichment values of 347.9 and 297 at 1% of sampling, respectively. However, in the case of FlexX-Pharm the total number of compounds docked successfully was very low. Moreover, the binding pose prediction analysis shows inconsistent results, the average rms deviation being on the order of $7.7 \text{ Å} \pm 4.4 \text{ Å}$. Therefore, we did not employ FlexX-Pharm for virtual screening. Enrichment of LigandFit hits sorted on the Jain scoring function is neither lower nor better than that for GLIDE. Flex-X, LigandFit hits sorted on DOCK scoring function, and Surflex did not report any active compounds at 1% of sampling; therefore, these methods were not suitable in this case. On the basis of this enrichment assessment, we decided to use GOLD and GLIDE for extensive virtual screening.

Virtual Screening. The virtual screening campaign conducted to screen for novel Eg5 inhibitors started with pharmacophore searching and docking. First, seven interaction-based pharmacophores (IBP) were searched against the ChemDiv database; detailed information about the hits obtained by pharmacophore-based screening is given in Table 4. All seven pharmacophore models coupled with shape query were searched in parallel. Every ligand conformation was fitted to the pharmacophore and ranked according to the highest fit values. The pharmacophore searching reduced the database to a large extent, as there were two criteria to satisfy. First, the database compounds had to pass the shape tolerance and had to match the pharmacophore features. The compounds were sorted according to their FitValues, which were always less than the number of features present in the pharmacophore. The 2UYM pharmacophore identified a compound with the highest fit-value of 4.383, as this pharmacophore has more features than others. In total, 1357 hits (0.2% of the entire database) were retrieved as a result of the IBP-based search, and these compounds entered the next level of filtering (Figure 2). The hit compounds were assumed to be in a bioactive conformation and considered as a suitable starting conformation for structure-based design. The IBP-based hits were docked to their corresponding structures by GOLD and GLIDE (6×2 trials). All compounds were successfully docked and sorted based on the Gold fitness or Glide score; molecules found in the top list

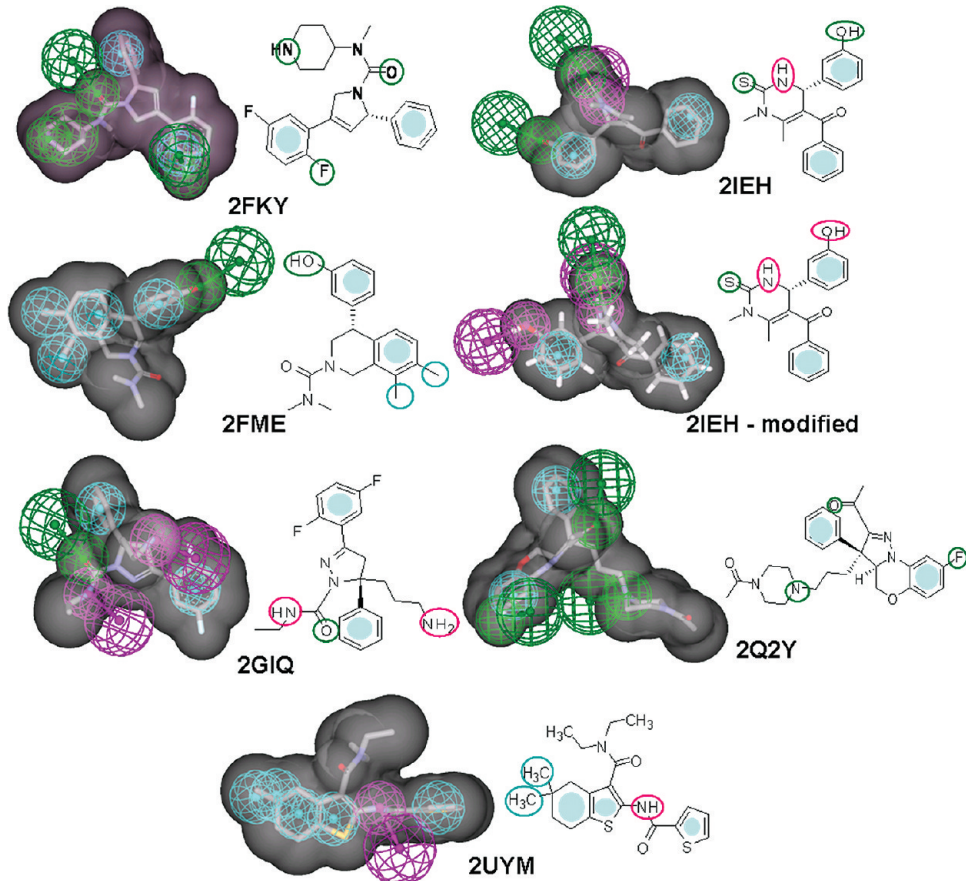


Figure 1. IBPs generated from six crystal structures. Hydrogen bond acceptors (green), hydrogen bond donors (magenta), and hydrophobic (cyan) features are displayed. The shapes of the compounds are represented in gray.

Table 1. Pharmacophore Models and Their Features with Location Constraint Radius (\AA)^a

pharmacophore (PDB ID)	sphere radius (\AA)					
	Ac.	Do.	Hy.	Ac.	Do.	Hy.
2FME	1	0	4	1.6, 2.2	—	1.6
2FKY	3	0	2	1.6, 2.2	—	1.6
2GIQ	1	2	2	1.6, 2.2	1.6, 2.2	1.6
2UYM	0	1	5	—	1.6, 2.2	1.6
2IEH	2	1	2	1.6, 2.2	1.6, 2.2	1.6
2IEH-modified	1	2	2	1.6, 2.2	1.6, 2.2	1.6
2Q2Y	3	0	2	1.6, 2.2	—	1.6

^aAc., acceptor; Do., donor; Hy., hydrophobic.

were considered and especially the compounds ranked at the top by both methods were given preference. From the top-ranked compounds, 100 (0.014% of the entire database) molecules were selected, from which 61 were further chosen based on visual analysis and diversity. Out of the 59 compounds obtained from vendors, 29 were reported with a purity of $\geq 95\%$ and 10 with a purity of $\geq 90\%$. Additional controls led to the elimination of 5 compounds with a purity of $\leq 90\%$. Vendors could not provide LC/MS data for the 15 compounds; however, we included those compounds for further evaluation. Finally, 54 compounds were subjected to in vitro and cell-based screening (Figure 2).

Verification of Novel Eg5 Inhibitors Identified by Virtual Screening. To unambiguously identify compounds that inhibit Eg5, we performed a range of in vitro and cell-based

assays. Initially, the whole set of compounds was tested in proliferation assays in two different tumor cell lines (DU145 and HT29). In parallel, we also measured the compounds for the inhibition of the basal Eg5 ATPase activity. Subsequently, the active compounds identified in these two assays were investigated for their potential to induce monoastrol spindles in HeLa cells, the well-described phenotype observed when Eg5 is inhibited. Finally, the specificity of the active compounds was tested in vitro against two additional human mitotic kinesins, HsKif5A and HsKif5C. The results are summarized in Table S5.

Inhibition of Tumor Cell Proliferation. The chemical structures of the 54 compounds tested in growth inhibition assays and the data for the inhibition of the Eg5 ATPase activity are summarized in Table S1 of the Supporting Information.

From the 54 compounds tested in human prostate (DU145) and human colon adenocarcinoma (HT29) cell lines, 18 compounds inhibited DU145 cells with GI_{50} values in the micromolar range, the most effective compound being **52**, which has a GI_{50} value of $8.7 \mu\text{M}$. In HT29 cells, 21 compounds showed an inhibitory effect, and **13** effectively inhibited the proliferation with a GI_{50} value of $0.7 \mu\text{M}$ but did not inhibit DU145 cells even at $100 \mu\text{M}$. Among the 54 compounds tested, 18 compounds commonly inhibited the two tumor cell lines, in which **52** was the most potent inhibitor for cell growth in both cell lines.

Inhibition of Basal Eg5 ATPase Activity. The 54 compounds were tested for the inhibition of the Eg5 ATPase activity in parallel to tumor proliferation assays. Six compounds were found to inhibit the basal ATPase activity of Eg5. Interestingly,

Table 2. RMSDs Calculated between Bioactive and Docked Conformations^a

Protein (PDB ID)	FlexX	FlexX-Pharm	Surflex	LigandFit	Gold	Glide
1X88	11.89	2.45	0.96	6.95	0.72	4.91
2FL6	16.65	7.33	7.47	4.84	6.99	1.91
2Q2Z	13.84	12.29	2.26	7.28	2.51	1.99
2UYI	14.25	8.56	7.76	7.5	1.77	0.92
1Q0B	9.97	6.11	2.93	6.56	2.53	4.89
1YRS	15.67	12.6	2.22	6.32	7.59	1.11
2FL2	12.01	4.15	2.01	1.8	0.79	5.04
2GM1	17.52	5.72	1.78	8.64	0.97	1.13
3CJO	18.9	10.52	1.77	8.71	1.35	3.64
2FKY	17.61	3.3	2.42	5.96	6.98	6.18
2FME	11.79	0.87	0.66	0.48	1	1.7
2GIQ	12.69	2.43	4.31	0.31	0.67	4.31
2IEH	12.42	14.69	2.35	7.65	6.17	2.46
2Q2Y	7.97	13.38	2.99	6.89	3.05	4.99
2UYM	17.11	6.39	1.74	7.89	1.22	1.77
2PG2	12.71	12.7	7.34	7.28	1.35	7.02
Mean (Å)	13.93	7.72	3.19	5.94	2.85	3.37
Std. dev. (Å)	3.06	4.49	2.31	2.71	2.54	1.98

RMSD < 5 Å | 5 Å < RMSD < 10 Å | 10 Å < RMSD < 15 Å | RMSD > 15 Å

^aA color code bar is given according to the RMSD range.

Table 3. Enrichment Calculations of 100 Eg5 Inhibitors Mixed with 2000 Decoys^{a,b}

database sampled	FlexX	FlexX-Pharm	Surflex	LigandFit (DOCK)	LigandFit (JAIN)	GLIDE	GOLD	ideal
1% EF	0	347.9	0	0	291	297	394	2100
5% EF	7.96	30.9	8	0	20	136	27.8	400
10% EF	13.9	8.2	6	0	12	53	13	100
compounds docked successfully	2071	167	2100	2037	2037	2077	1970	2100
TP	100	24	100	100	100	100	100	100
TN	1971	143	2000	1937	1937	1977	1870	2000

^aDatabase sampled at 1%, 5%, and 10% of hits. All docking results are summarized, and theoretical ideal enrichment factors are given for comparison.

^bTP, true positive; TN, true negative; EF, enrichment factor.

Table 4. Summarized Pharmacophore Screening Results^a

pharmacophore (PDB ID)	no. of hits	fit-value
2IEH	559	3.672–1.003
2FME	482	3.797–1.006
2UYM	169	4.383–1.034
2FKY	71	2.468–1.007
2GIQ	35	3.254–1.11
2Q2Y	32	2.741–1.008
2IEH modified	9	3.672–1.048

^aThe number of hits and their fit-values are shown.

compound 37 showed an IC₅₀ value in the submicromolar range, whereas most others inhibited Eg5 ATPase activity in the micromolar range. Compounds 30, 37, and 38 bear the thioxoimidazolidine core and were found to be potent Eg5 inhibitors in vitro, having IC₅₀ values of 0.58, 1.0, and 2.4 μM, respectively. Compound 37 is more potent than monastrol; however, there have been several monastrol analogues reported previously^{45,46} that have higher potency. Compound 24, bearing the quinazoline core, inhibits Eg5 ATPase activity with IC₅₀ value of 6.3 μM but did not inhibit growth in proliferation assays. Finally, compound 52 is a purine analogue showing weak potency (IC₅₀ = 41.5 μM). These compounds are novel Eg5 inhibitors and will need chemical optimization.

Four of the six compounds inhibiting Eg5 in vitro were also potent in both HT29 and DU145 tumor cell lines. Compound

52 is potent, having GI₅₀ values of 9.3 and 8.7 μM, respectively. However, 52 does not selectively inhibit Eg5, indicating that this compound might have additional cellular targets. Thioxoimidazolidine-based compounds 30, 37, and 38 are ~2 fold selective to colon over prostate cancer.

Specificity of Novel Eg5 Inhibitors. Compounds inhibiting Eg5 were tested on two additional human kinesins, HsKifSA and HsKifSC (kinesin-1 family), to investigate their specificity. Out of the six compounds tested, 52 was found to inhibit the two conventional kinesins, showing almost no selectivity over Eg5 (ratio of ~0.83). Other compounds are specific to Eg5 inhibition and did not inhibit HsKifSA or HsKifSC.

Phenotypic Analysis of Selected Eg5 Inhibitors. Our previous assays revealed a large discrepancy between compounds inhibiting growth in proliferation assays (21 compounds) and compounds inhibiting Eg5 in vitro (6 compounds), but we only identified 4 compounds that were active in both in vitro and cell-based assays. We therefore decided to employ a more Eg5-specific cell-based assay. The compounds exhibiting inhibition of the basal ATPase activity of Eg5 and antiproliferating activities in tumor cells were therefore tested for the ability to induce monoastral spindles. Monoastral spindles represent the characteristic phenotype of cells treated with known Eg5 inhibitors and is manifested by the nucleation of spindle MTs from the two centrosomes that failed to separate due to loss of Eg5 activity. At 25 μM, compounds 30 and 37 were capable of inducing a significant number of monoastral spindles, with 37 being

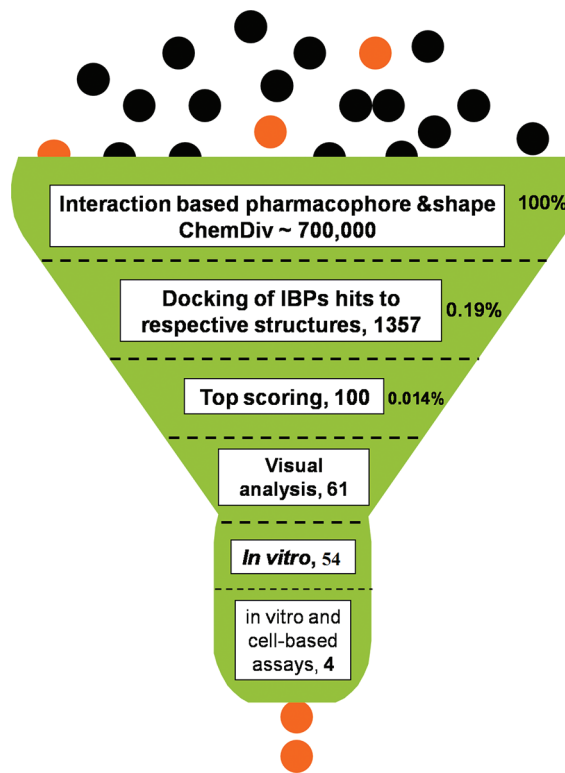


Figure 2. Schematic representation of the virtual screening protocol.

the most active compound compared to the rest. At 50 μM , compounds, 24 and 38 were also capable of inducing a significant number of monoastral spindles (Figure 3A,B), but they were less active compared to 37 (see Supporting Information Figure S1). At the highest concentration tested, 52 did not induce monoastral spindles.

Applying this assay, we were also capable of explaining why some of the compounds were active in proliferation assays but incapable of inhibiting Eg5 *in vitro*. Interestingly, cells treated with compound 18 exhibited bipolar spindles with misaligned chromosomes, a phenotype that is more compatible with a MT dynamics inhibitor rather than an Eg5 inhibitor (Figure 3A, middle upper panel). Cells treated with compound 20 at 25 μM after 8 h were stressed and no mitotic cells were detected whereas interphase cells exhibited cortical MT bundles (Figure 3A, right upper panel). Therefore, the antiproliferative properties of compounds 18 and 20 could be explained by their ability to either inhibit MT dynamics and/or being cytotoxic. Further analysis of the activities of 18 and 20 may be worth pursuing in the future.

Modeling-Derived Binding Mode of Novel Eg5 Inhibitors.

Three novel chemotypes targeting Eg5 have been identified, and their pharmacophore mapping and interactions in the allosteric pocket have been established. Figure 4 depicts the pharmacophore mapping of 37, 52, and 24 after being overlaid to 2Q2Y, 2FKY, or 2FME IBPs, respectively. The compound fit values are not very high because they bear distinct scaffolds compared to the pharmacophore template. On the other hand, these compounds possess critical features needed to inhibit Eg5. In the allosteric binding site there is a well-defined hydrophobic zone where the compounds establish hydrophobic interactions. Compound 37, which is the most potent inhibitor among the virtual screening hits, forms hydrogen bonds with Arg221 and Thr222 in addition to hydrophobic interactions (Figure 5a). In 37 the thioxoimidazolidine core oxygen and the

fluorine of the *p*-fluorobenzyl moiety interact with Arg221 and Thr222, respectively. The superposition of the crystal structure and the docked pose uncovers a possible binding mode. Strikingly, the predicted binding mode is closer to the crystal pose (Figure 5b), and the hydrophobic interactions are very similar while there is a slight difference in polar interactions. The 2Q2Y crystal structure-bound ligand establishes hydrogen bonds with Tyr211, whereas, in 37, this interaction is not present; hence, the binding mode is deviated. The purine-based compound 57 also forms well-defined hydrophobic interactions and two hydrogen bonds with Arg119 and Arg221 as shown in Figure 5c. 24 is a smaller compound than the two other scaffolds and could not establish hydrophobic interactions, similar to those of 37 or 52, and one hydrogen bond with the main chain carbonyl oxygen of Glu116 (Figure 5d).

CONCLUSIONS

The development of a successful virtual screening protocol by combining ligand- and structure-based models to identify novel Eg5 inhibitors has been described. On the basis of several available protein–ligand crystal structures, seven interaction IBP models were generated and applied to screen the ChemDiv database containing 0.7 million compounds, and only 59 compounds were retained as potential hits. Before docking the IBPs hits, the best docking methods were identified by predicting the bioactive conformation and subsequent enrichment calculations. This validation ensured the ability of various methods in predicting the correct binding mode and sensitivity toward the active compounds among the decoys. Finally, we found that GOLD and GLIDE outperformed other programs and therefore applied both methods to dock the IBP hits to their respective Eg5 structures.

From this screening approach, we understood that IBP can enhance docking results by providing the optimal initial conformation. The pharmacophore hits already retain the closest conformation to that of the bioactive molecule. Therefore, docking can generate several conformers from IBP hits, which are reasonably close to the bioactive form. Figure 6 depicts the superposition of pharmacophore and docking conformation of three chemotypes. Compound 37 has several rotatable groups, and therefore deviations occur; however, the fluorobenzene groups overlap, having an RMSD of 7.78 Å. In 52, docking and pharmacophore poses overlap closely with an RMSD of 2.53 Å. Compound 24 overlaps with an RMSD of 2.97 Å. The analysis shows that the pharmacophore is very efficient in conformation modeling especially for compounds having less rotatable groups.

To our knowledge, this is the first successful virtual screening strategy resulting in the identification of novel Eg5 inhibitors. Seven compounds bearing three different chemotypes were identified and found to inhibit human Eg5 at the enzymatic level having IC_{50} values in the submicromolar and micromolar range. We identified compound 37 as a potent agent specifically targeting Eg5, having an IC_{50} value of 0.58 μM and being capable of causing the monoastral spindle phenotype in HeLa cells as well as having appreciable growth inhibition in prostate and colon tumor cell lines. Similar results were obtained for its structural analogues 30 and 38. The hits identified by virtual screening can be a good starting point to develop more potent Eg5 inhibitors. Finally, this procedure will be employed to screen larger databases for new scaffolds inhibiting Eg5.

Table 5. Virtual Screening Hit Compounds Inhibiting Proliferation and ATPase Assay^{a,b}

Cmpd	Structure	IBP model	DU-145 GI ₅₀ (μM)	HT-29 GI ₅₀ (μM)	Inhibition Eg5 ATPase activity IC ₅₀ (μM) MIA (%)	Inhibition Kif5A ATPase activity IC ₅₀ (μM) MIA (%)	Inhibition Kif5C ATPase activity IC ₅₀ (μM) MIA (%)	Monoastral spindle phenotype at 25 μM inhibitor
18		2FME, 2UYM	>100	33.7 ± 2.7	n.i.	n.d.	n.d.	Multiple cells with misaligned chromosomes
19		2FKY	n.i.	n.i.	79.1 ± 22.4 (80)	n.i.	n.i.	n.m.s.o.
20		2IEH	21.0 ± 2.4	4.4 ± 0.3	n.i.	n.d.	n.d.	Interphase cells affected; MT bundles; no mitotic cells
22		2FKY, 2FME, 2IEH, 2Q2Y	41.2 ± 2.2	19.4 ± 4.0	n.i.	n.d.	n.d.	n.m.s.o.
24		2FME	n.i.	n.i.	6.3 ± 1.3 (60)	n.i.	n.i.	n.m.s.o. Monoastral spindles at 50 μM ~ 50% monoastral spindles
30		2Q2Y	34.3 ± 1.9	17.7 ± 2.8	1.0 ± 0.1 (60)	n.i.	n.i.	n.m.s.o. ~ 50% monoastral spindles
37		2Q2Y	31.0 ± 1	16.7 ± 1.1	0.6 ± 0.2 (80)	n.i.	n.i.	Most cells show monoastral spindles
38		2G1Q	42.3 ± 1.3	19.6 ± 3.9	2.4 ± 0.4 (60)	n.i.	n.i.	Very few monoastral spindles
52		2FKY	8.7 ± 2	9.3 ± 1.1	41.5 ± 4.9 (60)	~ 50	~ 50	n.m.s.o.

^a GI₅₀ values of the compounds calculated by MTT assay using prostate cancer (DU-145) and colon cancer (HT-29) cell lines. Compounds inhibiting the ATPase activity of Eg5, Kif5A, and Kif5C are also provided. STLC was used as a control. Some of the compounds are capable of causing various spindle phenotypes as summarized in the table. ^b IBP, interaction based pharmacophore; n.i., no inhibition; n.m.s.o., no monoastral spindles observed; MIA, maximum inhibition attained; n.d., not determined.

■ EXPERIMENTAL SECTION

Generation of Pharmacophore Models. Six crystal structures, namely, 2FKY,²⁴ 2IEH,⁴⁷ 2FME,⁴⁸ 2G1Q,²³ 2Q2Y,²⁷ and 2UYM,⁴⁹ were used to generate pharmacophore models. An IBP is a molecular framework that carries essential features responsible for a drug's (pharmacophore) biological activity. Interactions established by protein–ligand complexes are converted into features and combined with shape query. Discovery studio 2.5 (Accelrys, San Diego, CA) was used to visualize and convert the hydrogen bonding features into a pharmacophore query. The features related to hydrogen bonding have been obtained by measuring the distance between the hydrogen and the electronegative atom. The possible hydrogen bonds were considered up to a distance of 3.5 Å. In general, a single hydrogen bond is relatively weak; however, when

multiple hydrogen bonds are established around the ligand, they can significantly contribute to binding energy. LUDI⁵⁰ was used to model hydrophobic interactions of hydrophobic residues found in the active site, and for the purposes of our analysis, both aliphatic and aromatic interactions were treated as a hydrophobic interaction. There are many hydrophobic points generated in the active site; however, priority was given to the features that overlap the hydrophobic moiety of the ligand. LigandScout⁵¹ is a program that detects possible interactions between protein and ligand complexes automatically and converts the interaction into a pharmacophore model. FitValue is a score that measures how well the ligands fit the pharmacophore. The higher the fit score, the better the match. Perfect matching of database compounds with the pharmacophore centric point results in a high FitValue.

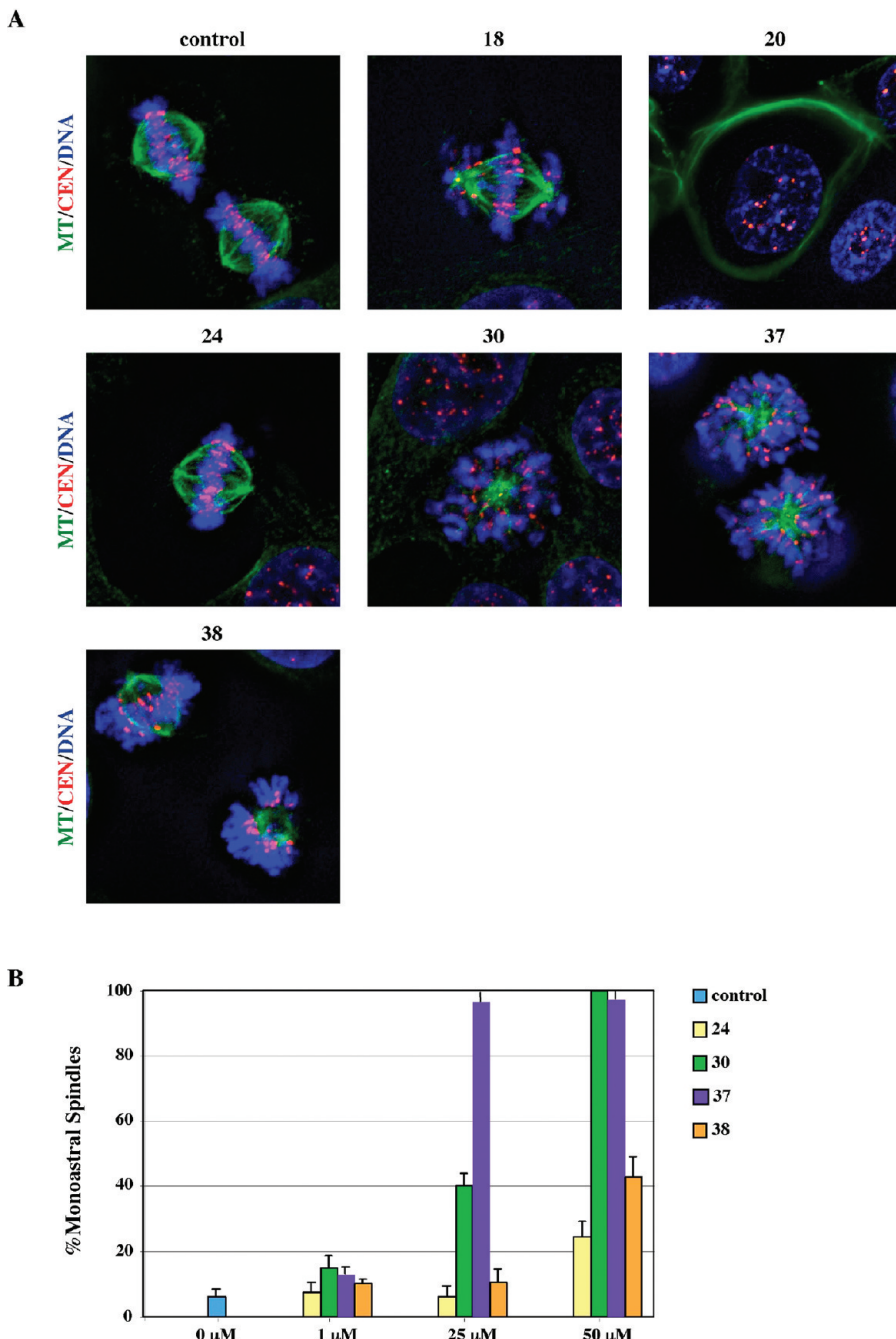


Figure 3. Phenotypic analysis of cells treated with selected small molecule inhibitors. (A) HeLa cells were treated with 25 μ M of each of the inhibitors for 8 h and then fixed and stained for indirect immunofluorescence microscopy: MTs (stained in green), centromeres (stained in red), and DNA (stained in blue). (B) The presence of bipolar spindles and monoastral spindles were scored in untreated control cells and at three different concentrations of each of the indicated inhibitors, and the % of monoastral spindles were determined and plotted as bar graphs.

Shape query is defined by a set of 3D coordinates, with a corresponding radius. Each of these points is the center of the atom, and the radius varies according to the atoms in the template molecule. The union of these points and spheres is referred to as shape query, and during database searching, each molecule in the database is converted to a similar volume. The two volumes are aligned, and the shape similarity is computed as the volume of the intersection divided by the union of the volume of the aligned shapes. Bioactive conformation shape is a true representation of the binding mode; therefore, shape-based searching can also be a useful approach in finding the appropriate binding mode of a compound. Ligand shape searching has been tested on various targets,⁵² and the importance of molecular shape in

ligand–receptor interactions has been demonstrated by the success of programs, such as ROCS in virtual screening, which identify similar molecules based on volume overlap.⁵³ The shape query can identify compounds having similar shape, area, and molecular weight. After merging of the interaction features and shape query, seven models were derived (Table 1).

Database Preparation. The ChemDiv database library containing 700 000 compounds was subjected to conformation modeling using the Catalyst module of Discovery studio 2.5. First, two-dimensional structures were converted into three-dimensional coordinates, and every compound in the database was enumerated into 250 or less conformations by fast searching method. The quality of pharmacophore

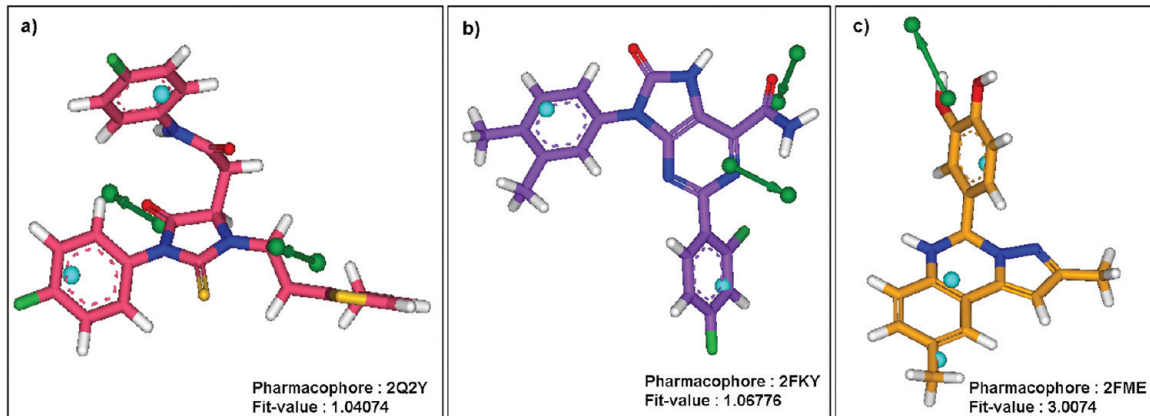


Figure 4. Pharmacophore mapping of the three chemotypes and FitValues of (a) 37, (b) 52, and (c) 24. During the pharmacophore mapping, any one of the features can be missed; therefore, the missed feature is not shown in the picture. Green arrows and spheres represent the acceptor feature, and cyan spheres correspond to hydrophobic feature. For the sake of clarity, the location constraint and the shape query are not displayed.

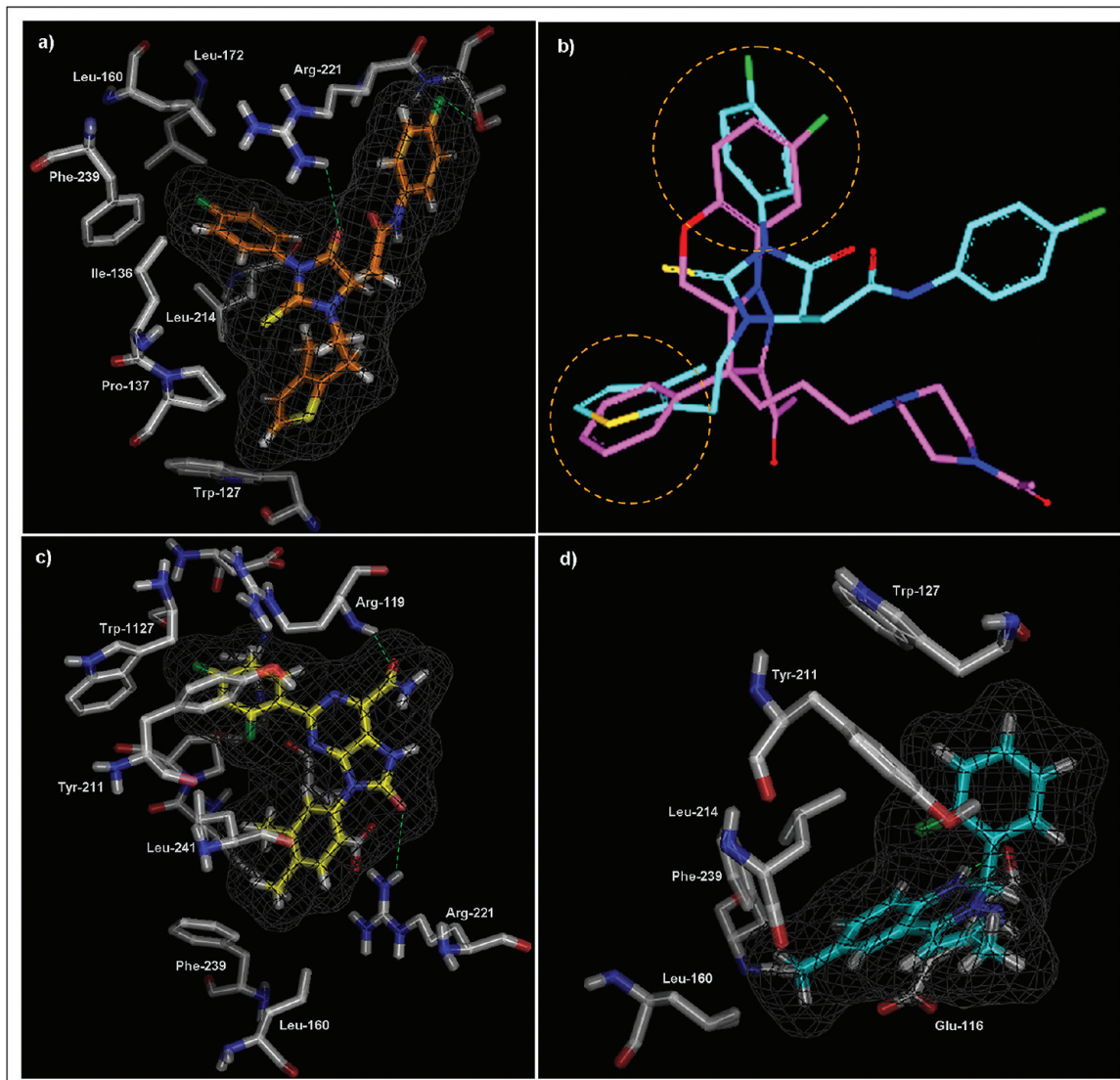


Figure 5. (a) Chemotype 1 (37) interaction with residues of the allosteric site. Orange and white colored sticks are ligand and protein, respectively. (b) Superposition of the docked pose (cyan) with the crystal structure of the 2Q2Y ligand (magenta). The circles represent the superposition of the hydrophobic moieties. (c) Chemotype 2 (52) interaction with the allosteric site. Yellow and white colored sticks are ligand and protein, respectively. (d) Chemotype 3 (24) interaction with the allosteric site. Cyan and white colored sticks are ligand and protein, respectively. The hydrogen bond is depicted with a green dotted line.

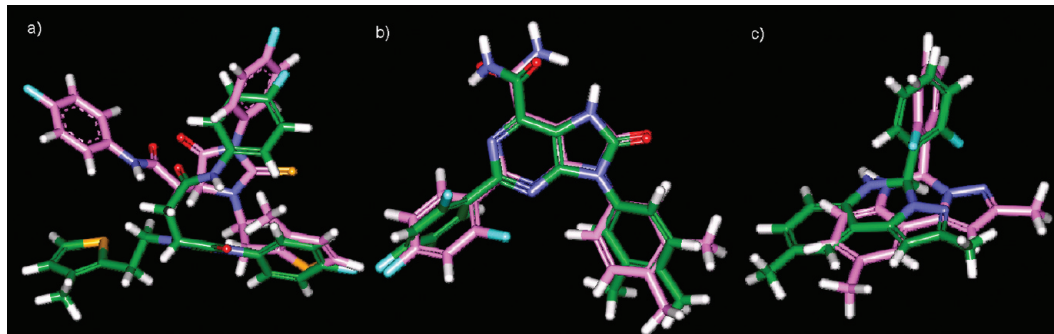


Figure 6. Superposition of pharmacophore (green stick) and docking (pink stick) conformations. (a) 37, (b) 52, and (c) 24.

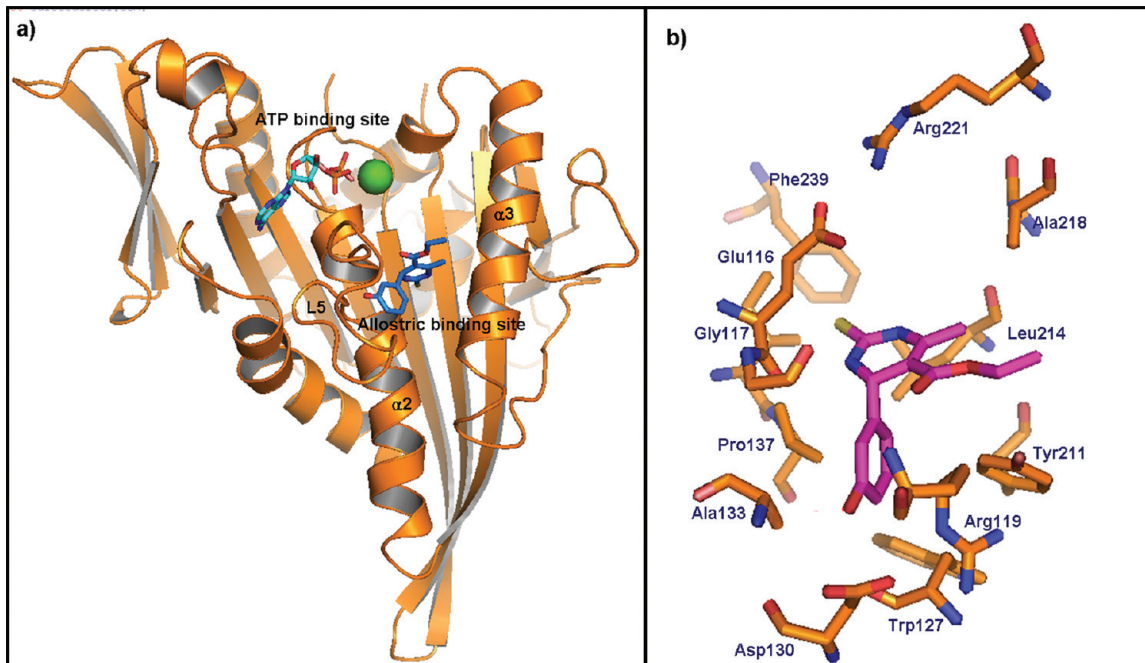


Figure 7. (a) Human Eg5 in complex with (S)-monastrol⁷ and Mg²⁺ADP. (b) Magnification of the allosteric inhibitor–binding pocket. Monastrol is colored in magenta with residues surrounding the inhibitor colored in orange.

searching is proportional to the conformation models present in the database. Conformation modeling depends on the molecule size, flexibility, and choice of algorithm. However, a search of the Multiconformer ChemDiv database by interaction features merged query can miss any one of the interaction features. Additionally, the shape query is mapped to the database candidate compound, and the hit compounds have to pass through the minimum 0.5 shape similarity tolerance.

Validation of the Docking Protocol. The conventional way of identifying a suitable docking protocol and scoring function is bioactive conformation prediction and rank ordering the top actives among the decoys. Bioactive conformation prediction ensures the ability of the conformation generation method of any docking program, and the enrichment calculation is a useful estimation to identify a suitable program that ranks true positives in the top level of database sampling. In total, 16 crystal structures of Eg5 that cocrystallized with various inhibitors (Table 2) were used in the assessment of targeting the allosteric ligand binding site. The allosteric site is composed of helix $\alpha 2$ /loop L5 and helix $\alpha 3$ (Figure 7a), and the active site residues are shown in Figure 7b. We have used five different docking methods for this purpose, FlexX,^{54–56} SurFlex,⁵⁷ GOLD,^{58–60} Glide,⁶¹ and LigandFit.⁶² In all these programs, van der Waals (vdW) and other critical parameters were not changed. Selection of docking programs was based on the availability. The detailed working principles behind each program and the docking set up are explained below.

FlexX and FlexX-Pharm. In FlexX,^{54–56} compounds are broken down into fragments and the base fragment called ligand core is selected automatically and placed in the active site by pose clustering techniques. The rest of the ligand fragments are grown incrementally from other fragments at the active site. Conformational flexibility of the ligand is addressed by multiple conformations generated to the fragments at the ligand building stage. The binding energy is estimated by a scoring function. FlexX-Pharm⁶³ also follows the above specified procedure; in addition, it allows the definition of pharmacophore constraints. Therefore, important protein–ligand interaction constraints can direct FlexX docking. Protein hydrogen atoms were merged to satisfy the valence; AMBER FF99 charges were adopted to the protein and minimized with the Tripos force field to reach the gradient of 0.05 kcal/mol using Sybyl 8.0. The active site was specified based on the active-site residues such as Glu116–Arg119, Trp127, Asp130, Ala133, Gly134, Ile136–Arg138, Leu214–Ala219, Arg221, and Phe239. Hydrogen bond constraints were defined as observed in many experimentally determined structures: the main chain carbonyl of Trp127 is frequently found to act as a hydrogen bond acceptor whereas the main chain nitrogen of Arg119 acts as a donor in most of the cases.

Surflex. This method, different from other docking methods, combines Hammerhead's empirical scoring function with the molecular similarity method.⁵⁷ The active site is represented as a negative image

called protomol, in which steric/hydrophobic (CH_4), hydrogen bond donor (N–H), and acceptor (C=O) probes are used to access the favorable interaction. The best interaction points are called sticky spots and used to align the ligand fragment and also to provide the direction to grow the fragments. The protein structures prepared for FlexX docking are used in this case, and the protomol active site is defined based on the above-mentioned residues.

Gold. GOLD performs automated ligand docking that uses a genetic algorithm (GA) to explore full ligand flexibility and partial receptor flexibility. Hydrogen bond-encoded GA directs the proper binding mode identification.^{58–60} Each molecule is encoded as a chromosome in a genetic algorithm, the genetic operators such as cross over, and mutations evolve a new conformation. Protein structures were prepared by Herms visualization tool adding hydrogens and deleting water and ligand molecules. The active-site was defined based on a 10 Å radius surrounding the ligand. In the genetic algorithm search, a population was set to minimum 100 and maximum 100 000 individual operations. A maximum of 10 conformations was generated when the RMSD of the top three scoring poses was more than 1.5 Å.

Glide. GLIDE (grid-based ligand docking with energetics)⁶¹ searches for the possible location of ligands in several steps. First, the receptor shape and properties are represented on a grid by different fields. A set of initial ligand conformations is generated, and the lowest energy conformer is retained for further screening. Initial screens are performed over the entire phase space available to the ligand to locate promising ligand poses. The best pose conformation energy is minimized at the receptor environment with the OPLS-AA force field⁶⁴ in conjunction with the distance-dependent dielectric model. Finally, Monte Carlo simulation is conducted between the three to six lowest energy poses of the previous step to explore nearby torsional minima. To score the ligand pose, Glidescore is used, which is an expanded version of ChemScore.⁶⁵ Prior to docking, the crystal structures were prepared, adding hydrogens, assigning bond orders, and minimizing hydrogens. Shape and various properties of the receptor are represented in a grid cell by various fields. From the ligand centroid, a 20 Å slider was set to cover the entire allosteric site.

LigandFit. LigandFit is a shape-based docking method.⁶² An automated cavity detection algorithm is employed to detect invaginations in the protein as an active site region. A sophisticated Monte Carlo conformation search generates a ligand pose along with the active site shape. Further grid-based energy minimization of the ligand pose is applied to determine the protein–ligand interaction energy. Prior to docking the protein structures were minimized for 100 cycles of the steepest descent, followed by 500 cycles of conjugate gradient. The binding site was defined based on the volume occupied by a bound ligand. The algorithm detected the cavity expelling the ligand, and the binding site was expanded to several points to cover the whole allosteric pocket.

Prediction of Bioactive Conformations. Protein-bound ligand structures were extracted, hydrogen atoms were added, and charges were calculated using the Gasteiger–Marsili method and slightly minimized to optimize the newly added hydrogen atoms using Sybyl (<http://tripos.com>). Ligands were docked to the respective protein structures using the five docking protocols. The first ranked pose was considered as a candidate conformation to compare with the experimentally derived conformation by calculating the RMSD.

Enrichment Calculations. Enrichment calculation has been used as a reliable metric to benchmark the methods used in rational drug design.^{66–70} Here we used the enrichment calculation to quantitatively assess the performance of various docking protocols. We used 100 Eg5 inhibitors collected from the BindingDB⁷¹ database, and only compounds having IC_{50} or K_i values less than or equal to 1 μM were considered as active compounds. The physicochemical properties observed in the active compounds (Table 6) were used to filter decoys compounds from the ZINCDB⁷² database. The main purpose of having actives mixed with decoys is to reflect the realistic situation of virtual screening. The docking hits obtained by various protocols were considered at 1%, 5%, and 10% of sampling, and enrichments were calculated accordingly. Enrichment calculation was performed as follows $\text{EF} = (\text{N}_{\text{active}}(\%) \times N_{\text{all}}) / (N(\%) \times N_{\text{active}})$, where $N_{\text{active}}(\%)$ is the percentage of actives found in x%,

Table 6. Physicochemical Properties Observed for Eg5 Ligands and Their Range Used in Decoy Preparation

properties	range
AlogP	0.994–6.206
molecular weight	280.364–529.444
hydrogen bond acceptors	1–6
hydrogen bond donors	0–3
rota table bonds	1–11
polar surface area	3.24–128.66

N_{all} is the number of compounds used in the test, $N(\%)$ is the x% of the compounds used in the calculation of EF(%), N_{active} is the number of all actives used in the calculation of the enrichment factor, and x% corresponds to 1%, 5%, and 10% sampling.

Virtual Screening. All seven IBPs were used in a virtual screen of the ChemDiv (0.7 million compounds). While searching the pharmacophore against the database, we have modified the parameter so that a pharmacophore can find compounds either matching all the features or any one of the features can be omitted. The possibility to find compounds having all the pharmacophore features is relatively low. The fast searching algorithm implemented in Catalyst was used to search the database. In principle, database searching is performed based on the feature mapping with every compound in the database and sorting according to the higher FitValue scores. All the pharmacophore hit compounds were further subjected to structure-based filtering.

We used GOLD and GLIDE as a combined secondary filter to prioritize the compounds for in vitro screening. All IBPs hits were docked to their respective six crystal structures by both docking methods. Hit compounds were sorted based on the docking score, and the top ranking compounds were considered. In the sorted list, priority was given to the compounds that establish patterns of interaction similar to that of respective bioactive conformations. Finally, the hit compounds were purchased and subjected to various biological assays as explained below. Separate LC/MS assessment was carried out with ChemDiv for the hit compounds in order to verify the purity of the compounds, in which 15 compounds do not have sufficient samples and 5 compounds have purity less than 90%. Therefore, the compounds having an impurity percentage less than 10% will be considered for chemical modification.

MTT Assays. Cytotoxic activities of the hits were investigated against human cancer cell lines using the MTT assay.⁷³ Human colon adenocarcinoma (HT-29) and human prostate cancer (DU145) cell lines were obtained from the Korean Cell Line Bank, Seoul National University. Both cell lines were grown in RPMI 1640 (Gibco BRL) supplemented with 10% (v/v) heat-inactivated fetal bovine serum (FBS) and maintained at 37 °C in a humidified atmosphere with 5% CO_2 . The cells (3×10^3 cells/well) were seeded into 96-well plates. Various sample concentrations (hit compounds) were added to each well in duplicate and then incubated at 37 °C with 5% CO_2 for two days such that cells are in the exponential growth phase at the time of drug addition. Fifteen microliters of the Dye Solution (Promega, CellTiter96) was added to each well and incubated at 37 °C for up to 4 h in a humidified, 5% CO_2 atmosphere. After incubation, 100 μL of the Solubilization Solution/Stop Mix (Promega, CellTiter96) was added to each well. The plate was allowed to stand overnight in a sealed container with a humidified atmosphere at room temperature to completely solubilize the formazan crystals. The optical density was measured using a microplate reader (Versamax, Molecular Devices) at a wavelength of 570 nm, and the effective concentration was expressed as GI_{50} .

Inhibition of Eg5 ATPase Activity. All experiments were performed at 25 °C using a 96-well Sunrise photometer (Tecan, Maennedorf, Switzerland) at a final volume of 100 μL per well. Steady-state ATPase rates were measured using the pyruvate kinase/lactate dehydrogenase-linked assay in buffer A2SA [25 mmol/L potassium ACES (pH 6.9), 2 mmol/L magnesium acetate, 2 mmol/L potassium EGTA, 0.1 mmol/L potassium EDTA, 1 mmol/L β -mercaptoethanol]. The basal ATPase activity was measured using 200 nM Eg5_{2–368}. For optimal inhibitor solubility, the assays were performed in the presence of up to 2.0% DMSO. The data were analyzed using Kaleidagraph 3.0 (Synergy Software,

Reading, PA) and Microsoft Excel to obtain IC₅₀ values. STLC¹⁹ was used as a positive control. When necessary, the inhibitory concentrations were adapted, depending on the initial IC₅₀ value. Each inhibitory concentration was measured in triplicate, and averaged data points \pm SD are shown. The specificity of the Eg5 inhibitors was tested using two other members of the kinesin superfamily, HsKif5A and HsKif5C.

Immunofluorescence Microscopy. HeLa cells were grown in D-MEM (Gibco BRL; Paisley, UK), supplemented with 10% fetal calf serum (Hyclone) on poly-D-lysine (Sigma-Aldrich)-coated 12-mm diameter glass coverslips in 24-well plates. Cells were seeded and allowed to adhere for at least 36 h before drug addition. Drugs were diluted appropriately in medium from 25 mM stocks in 100% DMSO and then added to the cells. Following 8 h incubation with drugs, cells were fixed by incubation in 2% paraformaldehyde (20 min at 37 °C) and permeabilized with 0.2% Triton X-100 in PBS for 3 min before being incubated with primary and stained with secondary antibodies. Cells were stained with anti- β -tubulin monoclonal antibodies (Sigma) at 400-fold dilution and human autoimmune antigen-recognizing centromeres (Immunovision) at 1000-fold dilution for 1 h and then with Alexa fluor 488-conjugated goat antimouse and Alexa fluor 568-conjugated goat antihuman secondary antibodies (Invitrogen) at 300-fold dilution for 30 min; DNA was detected with 4',6-diamidino-2-phenylindole dihydrochloride (DAPI) with VECTASHIELD mounting medium. The percentage of mitotic cells with monoastral spindles present in treated cells was calculated over the total number of cells in mitosis counted after 8 h incubation with drugs. Images were collected with an inverted Olympus IX81 epifluorescence motorized microscope equipped with a motorized piezo stage (Ludl Electronic Products, Hawthorne, NY) and a Retiga-SRV CCD camera (QImaging) driven by VOLOCITY software (Improvision) with a binning of 1, using a PlanApo 60 \times NA1.42 objective (Olympus). Images were processed in Photoshop version 7.0 (Adobe) and assembled in CANVAS version 8.0 (Denaba Systems).

■ ASSOCIATED CONTENT

S Supporting Information

Additional information as noted in the text. This material is available free of charge via the Internet at <http://pubs.acs.org>.

■ AUTHOR INFORMATION

Corresponding Author

*Tel: +82 2 958 5185; fax: +82 2 958 5189; e-mail: anpae@kist.re.kr.

Notes

The authors declare no competing financial interest.

■ ACKNOWLEDGMENTS

We thank Marta Kozlowska (The Beatson Institute for Cancer Research) for providing us with purified Kif5A and Kif5C kinesin motor proteins. We are grateful to Cancer Research UK for financial support. D.S. is supported by La Ligue Contre le Cancer.

■ ABBREVIATIONS USED

IBP, interaction-based pharmacophore; KSP, kinesin spindle protein; MTs, microtubules; RMSD, root mean square deviation; PDB, protein data bank; VS, virtual screening

■ REFERENCES

- Miki, H.; Okada, Y.; Hirokawa, N. Analysis of the kinesin superfamily: insights into structure and function. *Trends Cell Biol.* 2005, 15 (9), 467–476.
- Cochran, J. C.; Krzysiak, T. C.; Gilbert, S. P. Pathway of ATP hydrolysis by monomeric kinesin Eg5. *Biochemistry* 2006, 45 (40), 12334–12344.
- Sarli, V.; Giannis, A. Targeting the kinesin spindle protein: Basic principles and clinical implications. *Clin. Cancer Res.* 2008, 14 (23), 7583–7587.
- Kashina, A. S.; Baskin, R. J.; Cole, D. G.; Wedaman, K. P.; Saxton, W. M.; Scholey, J. M. A bipolar kinesin. *Nature* 1996, 379 (6562), 270–272.
- Kapitein, L. C.; Peterman, E. J. G.; Kwok, B. H.; Kim, J. H.; Kapoor, T. M.; Schmidt, C. F. The bipolar mitotic kinesin Eg5 moves on both microtubules that it crosslinks. *Nature* 2005, 435 (7038), 114–118.
- Tao, W. K.; South, V. J.; Diehl, R. E.; Davide, J. P.; Sepp-Lorenzino, L.; Fraley, M. E.; Arrington, K. L.; Lobell, R. B. An inhibitor of the kinesin spindle protein activates the intrinsic apoptotic pathway independently of p53 and de novo protein synthesis. *Mol. Cell Biol.* 2007, 27 (2), 689–698.
- Bacher, G.; Beckers, T.; Emig, P.; Klenner, T.; Kutscher, B.; Nickel, B. New small-molecule tubulin inhibitors. *Pure Appl. Chem.* 2001, 73 (9), 1459–1464.
- Jordan, M. A.; Wendell, K.; Gardiner, S.; Derry, W. B.; Copp, H.; Wilson, L. Mitotic block induced in HeLa cells by low concentrations of paclitaxel (Taxol) results in abnormal mitotic exit and apoptotic cell death. *Cancer Res.* 1996, 56 (4), 816–825.
- Chen, J. G.; Yang, C. P. H.; Cammer, M.; Horwitz, S. B. Gene expression and mitotic exit induced by microtubule-stabilizing drugs. *Cancer Res.* 2003, 63 (22), 7891–7899.
- Rowinsky, E. K.; Eisenhauer, E. A.; Chaudhry, V.; Arbuck, S. G.; Donehower, R. C. Clinical toxicities encountered with paclitaxel (Taxol(R)). *Semin. Oncol.* 1993, 20 (4), 1–15.
- Kuppens, I. E. L. M. Current state of the art of new tubulin inhibitors in the clinic. *Curr. Clin. Pharmacol.* 2006, 1 (1), 57–70.
- Sakowicz, R.; Finer, J. T.; Beraud, C.; Crompton, A.; Lewis, E.; Fritsch, A.; Lee, Y.; Mak, J.; Moody, R.; Turincio, R.; Chabala, J. C.; Gonzales, P.; Roth, S.; Weitman, S.; Wood, K. W. Antitumor activity of a kinesin inhibitor. *Cancer Res.* 2004, 64 (9), 3276–3280.
- Lad, L.; Luo, L.; Carson, J. D.; Wood, K. W.; Hartman, J. J.; Copeland, R. A.; Sakowicz, R. Mechanism of inhibition of human KSP by ispinesib. *Biochemistry* 2008, 47 (11), 3576–3585.
- Cox, C. D.; Coleman, P. J.; Breslin, M. J.; Whitman, D. B.; Garbaccio, R. M.; Fraley, M. E.; Buser, C. A.; Walsh, E. S.; Hamilton, K.; Schaber, M. D.; Lobell, R. B.; Tao, W.; Davide, J. P.; Diehl, R. E.; Abrams, M. T.; South, V. J.; Huber, H. E.; Torrent, M.; Prueksaritanont, T.; Li, C.; Slaughter, D. E.; Mahan, E.; Fernandez-Metzler, C.; Yan, Y.; Kuo, L. C.; Kohl, N. E.; Hartman, G. D. Kinesin spindle protein (KSP) inhibitors. 9. Discovery of (2S)-4-(2,5-difluorophenyl)-N-[(3R,4S)-3-fluoro-1-methylpiperidin-4-yl]-2-(hydroxymethyl)-N-methyl-2-phenyl-2,5-dihydro-1H-pyrrole-1-carboxamide (MK-0731) for the treatment of taxane-refractory cancer. *J. Med. Chem.* 2008, 51 (14), 4239–4252.
- Kim, K. H.; Xie, Y. H.; Tytler, E. M.; Woessner, R.; Mor, G.; Alvero, A. B. KSP inhibitor ARRY-520 as a substitute for Paclitaxel in Type I ovarian cancer cells. *J. Transl. Med.* 2009, 7, 63.
- Carter, B. Z.; Mak, D. H.; Schober, W. D.; Woessner, R.; Gross, S.; Harris, D.; Estrov, Z.; Andreeff, M. Inhibition of KSP by ARRY-520 induces cell cycle block and cell death, via the mitochondrial pathway in AML cells. *Blood* 2007, 110 (11), 819a–819a.
- Carter, B. Z.; Mak, D. H.; Woessner, R.; Gross, S.; Schober, W. D.; Estrov, Z.; Kantarjian, H.; Andreeff, M. Inhibition of KSP by ARRY-520 induces cell cycle block and cell death via the mitochondrial pathway in AML cells. *Leukemia* 2009, 23 (10), 1755–1762.
- Mayer, T. U.; Kapoor, T. M.; Haggarty, S. J.; King, R. W.; Schreiber, S. L.; Mitchison, T. J. Small molecule inhibitor of mitotic spindle bipolarity identified in a phenotype-based screen. *Science* 1999, 286 (5441), 971–974.
- Skoufias, D. A.; DeBonis, S.; Saoudi, Y.; Lebeau, L.; Crevel, I.; Cross, R.; Wade, R. H.; Hackney, D.; Kozielski, F. S-Trityl-L-cysteine is a reversible, tight binding inhibitor of the human kinesin Eg5 that specifically blocks mitotic progression. *J. Biol. Chem.* 2006, 281 (26), 17559–17569.
- Coleman, P. J.; Schreler, J. D.; Cox, C. D.; Fraley, M. E.; Garbaccio, R. M.; Buser, C. A.; Walsh, E. S.; Hamilton, K.; Lobell,

- R. B.; Rickert, K.; Tao, W. K.; Diehl, R. E.; South, V. J.; Davide, J. P.; Kohl, N. E.; Yan, Y. W.; Kuo, L.; Prueksaritanont, T.; Li, C. Z.; Mahan, E. A.; Fernandez-Metzler, C.; Salata, J. J.; Hartman, G. D. Kinesin spindle protein (KSP) inhibitors. Part 6: Design and synthesis of 3,5-diaryl-4,5-dihydropyrazole amides as potent inhibitors of the mitotic kinesin KSP. *Bioorg. Med. Chem. Lett.* **2007**, *17* (19), 5390–5395.
- (21) Cox, C. D.; Breslin, M. J.; Brenda, J. M.; Coleman, P. J.; Buser, C. A.; Walsh, E. S.; Hamilton, K.; Huber, H. E.; Kohl, N. E.; Torrent, M.; Yan, Y. W.; Kuo, L. C.; Hartman, G. D. Kinesin spindle protein (KSP) inhibitors. Part 1: The discovery of 3,5-diaryl-4,5-dihydropyrazoles as potent and selective inhibitors of the mitotic kinesin KSP. *Bioorg. Med. Chem. Lett.* **2005**, *15* (8), 2041–2045.
- (22) Cox, C. D.; Breslin, M. J.; Whitman, D. B.; Coleman, P. J.; Garbaccio, R. M.; Fraley, M. E.; Zrada, M. M.; Buser, C. A.; Walsh, E. S.; Hamilton, K.; Lobell, R. B.; Tao, W. K.; Abrams, M. T.; South, V. J.; Huber, H. E.; Kohl, N. E.; Hartman, G. D. Kinesin spindle protein (KSP) inhibitors. Part V: Discovery of 2-propylamino-2,4-diaryl-2,5-dihydropyrroles as potent, water-soluble KSP inhibitors, and modulation of their basicity by beta-fluorination to overcome cellular efflux by P-glycoprotein. *Bioorg. Med. Chem. Lett.* **2007**, *17* (10), 2697–2702.
- (23) Cox, C. D.; Torrent, M.; Breslin, M. J.; Mariano, B. J.; Whitman, D. B.; Coleman, P. J.; Buser, C. A.; Walsh, E. S.; Hamilton, K.; Schaber, M. D.; Lobell, R. B.; Tao, W. K.; South, V. J.; Kohl, N. E.; Yan, Y. W.; Kuo, L. C.; Prueksaritanont, T.; Slaughter, D. E.; Li, C. Z.; Mahan, E.; Lu, B.; Hartman, G. D. Kinesin spindle protein (KSP) inhibitors. Part 4: Structure-based design of 5-alkylamino-3,5-diaryl-4,5-dihydropyrazoles as potent, water-soluble inhibitors of the mitotic kinesin KSP. *Bioorg. Med. Chem. Lett.* **2006**, *16* (12), 3175–3179.
- (24) Fraley, M. E.; Garbaccio, R. M.; Arrington, K. L.; Hoffman, W. F.; Tasber, E. S.; Coleman, P. J.; Buser, C. A.; Walsh, E. S.; Hamilton, K.; Fernandes, C.; Schaber, M. D.; Lobell, R. B.; Tao, W. K.; South, V. J.; Yan, Y. W.; Kuo, L. C.; Prueksaritanont, T.; Shu, C.; Torrent, M.; Heimbrook, D. C.; Kohl, N. E.; Huber, H. E.; Hartman, G. D. Kinesin spindle protein (KSP) inhibitors. Part 2: The design, synthesis, and characterization of 2,4-diaryl-2,5-dihydropyrrole inhibitors of the mitotic kinesin KSP. *Bioorg. Med. Chem. Lett.* **2006**, *16* (7), 1775–1779.
- (25) Garbaccio, R. M.; Fraley, M. E.; Tasber, E. S.; Olson, C. M.; Hoffman, W. F.; Arrington, K. L.; Torrent, M.; Buser, C. A.; Walsh, E. S.; Hamilton, K.; Schaber, M. D.; Fernandes, C.; Lobell, R. B.; Tao, W. K.; South, V. J.; Yan, Y. W.; Kuo, L. C.; Prueksaritanont, T.; Slaughter, D. E.; Shu, C.; Heimbrook, D. C.; Kohl, N. E.; Huber, H. E.; Hartman, G. D. Kinesin spindle protein (KSP) inhibitors. Part 3: Synthesis and evaluation of phenolic 2,4-diaryl-2,5-dihydropyrroles with reduced hERG binding and employment of a phosphate prodrug strategy for aqueous solubility. *Bioorg. Med. Chem. Lett.* **2006**, *16* (7), 1780–1783.
- (26) Garbaccio, R. M.; Tasber, E. S.; Neilson, L. A.; Coleman, P. J.; Fraley, M. E.; Olson, C.; Bergman, J.; Torrent, M.; Buser, C. A.; Rickert, K.; Walsh, E. S.; Hamilton, K.; Lobell, R. B.; Tao, W. K.; South, V. J.; Diehl, R. E.; Davide, J. P.; Yan, Y. W.; Kuo, L. C.; Li, C. Z.; Prueksaritanont, T.; Fernandez-Metzler, C.; Mahan, E. A.; Slaughter, D. E.; Salata, J. J.; Kohl, N. E.; Huber, H. E.; Hartman, G. D. Kinesin spindle protein (KSP) inhibitors. Part 7: Design and synthesis of 3,3-disubstituted dihydropyrazolobenzoxazines as potent inhibitors of the mitotic kinesin KSP. *Bioorg. Med. Chem. Lett.* **2007**, *17* (20), S671–S676.
- (27) Roecker, A. J.; Coleman, P. J.; Mercer, S. P.; Schreier, J. D.; Buser, C. A.; Walsh, E. S.; Hamilton, K.; Lobell, R. B.; Tao, W. K.; Diehl, R. E.; South, V. J.; Davide, J. P.; Kohl, N. E.; Yan, Y. W.; Kuo, L. C.; Li, C. Z.; Fernandez-Metzler, C.; Mahan, E. A.; Prueksaritanont, T.; Hartman, G. D. Kinesin spindle protein (KSP) inhibitors. Part 8: Design and synthesis of 1,4-diaryl-4,5-dihydropyrazoles as potent inhibitors of the mitotic kinesin KSP. *Bioorg. Med. Chem. Lett.* **2007**, *17* (20), S677–S682.
- (28) Chu, Q. S.; Holen, K. D.; Rowinsky, E. K.; Wilding, G.; Volkman, J. L.; Orr, J. B.; Williams, D. D.; Hodge, J. P.; Sabry, J. Phase I trial of novel kinesin spindle protein (KSP) inhibitor SB-715992IV Q 21 days. *J. Clin. Oncol.* **2004**, *22* (14S), 2078.
- (29) Blagden, S. P.; Molife, L. R.; Seebaran, A.; Payne, M.; Reid, A. H. M.; Protheroe, A. S.; Vasist, L. S.; Williams, D. D.; Bowen, C.; Kathman, S. J.; Hodge, J. P.; Dar, M. M.; De Bono, J. S.; Middleton, M. R. A phase I trial of ipinesib, a kinesin spindle protein inhibitor, with docetaxel in patients with advanced solid tumours. *Br. J. Cancer* **2008**, *98* (5), 894–899.
- (30) Chin, D. N.; Chuaqui, C. E.; Singh, J. Integration of virtual screening into the drug discovery process. *Mini-Rev. Med. Chem.* **2004**, *4* (10), 1053–1065.
- (31) Stahura, F. L.; Bajorath, J. Virtual screening methods that complement HTS. *Comb. Chem. High Throughput Screening* **2004**, *7* (4), 259–269.
- (32) Bender, A.; Mussa, H. Y.; Glen, R. C.; Reiling, S. Similarity searching of chemical databases using atom environment descriptors (MOLPRINT 2D): Evaluation of performance. *J. Chem. Inf. Comput. Sci.* **2004**, *44* (5), 1708–1718.
- (33) van Geerestein, V. J.; Perry, N. C.; Grootenhuis, P. D. J.; Haasnoot, C. A. G. 3D Database searching on the basis of ligand shape using the prototype method. *Tetrahedron Comput. Methodol.* **1990**, *3* (6, Part 3), 595–613.
- (34) Langer, T.; Wolber, G. Pharmacophore definition and 3D searches. *Drug Discovery Today: Technol.* **2004**, *1* (3), 203–207.
- (35) Cheeseright, T. J.; Mackey, M. D.; Melville, J. L.; Vinter, J. G. FieldScreen: Virtual screening using molecular fields. Application to the DUD data set. *J. Chem. Inf. Model.* **2008**, *48* (11), 2108–2117.
- (36) Hansch, C.; Muir, R. M.; Fujita, T.; Maloney, P. P.; Geiger, F.; Streich, M. The correlation of biological activity of plant growth regulators and chloromycetin derivatives with hammett constants and partition coefficients. *J. Am. Chem. Soc.* **1963**, *85* (18), 2817–2824.
- (37) Lipinski, C. A.; Lombardo, F.; Dominy, B. W.; Feeney, P. J. Experimental and computational approaches to estimate solubility and permeability in drug discovery and development settings. *Adv. Drug Delivery Rev.* **1997**, *23* (1–3), 3–25.
- (38) Lengauer, T.; Rarey, M. Computational methods for biomolecular docking. *Curr. Opin. Struct. Biol.* **1996**, *6* (3), 402–406.
- (39) Liu, F.; You, Q. D.; Chen, Y. D. Pharmacophore identification of KSP inhibitors. *Bioorg. Med. Chem. Lett.* **2007**, *17* (3), 722–726.
- (40) Jiang, C.; Chen, Y. D.; Wang, X. J.; You, Q. D. Docking studies on kinesin spindle protein inhibitors: an important cooperative 'minor binding pocket' which increases the binding affinity significantly. *J. Mol. Model.* **2007**, *13* (9), 987–992.
- (41) Chen, Z.; Tian, G. H.; Wang, Z.; Jiang, H. L.; Shen, J. S.; Zhu, W. L. Multiple pharmacophore models combined with molecular docking: A reliable way for efficiently identifying novel PDE4 inhibitors with high structural diversity. *J. Chem. Inf. Model.* **2010**, *50* (4), 615–625.
- (42) Wang, H. W.; Duffy, R. A.; Boykow, G. C.; Chackalamannil, S.; Madison, V. S. Identification of novel cannabinoid CB1 receptor antagonists by using virtual screening with a pharmacophore model. *J. Med. Chem.* **2008**, *51* (8), 2439–2446.
- (43) Markt, P.; Feldmann, C.; Rollinger, J. M.; Raduner, S.; Schuster, D.; Kirchmair, J.; Distinto, S.; Spitzer, G. M.; Wolber, G.; Laggner, C.; Altmann, K. H.; Langer, T.; Gertsch, J. Discovery of novel CB2 receptor ligands by a pharmacophore-based virtual screening workflow. *J. Med. Chem.* **2009**, *52* (2), 369–378.
- (44) Bernstein, F. C.; Koetzle, T. F.; Williams, G. J. B.; Meyer, E. F.; Brice, M. D.; Rodgers, J. R.; Kennard, O.; Shimanouchi, T.; Tasumi, M. The protein data bank: A computer-based archival file for macromolecular structures. *Arch. Biochem. Biophys.* **1978**, *185* (2), 584–591.
- (45) Kaan, H. Y. K.; Ulaganathan, V.; Hackney, D. D.; Kozielski, F. An allosteric transition trapped in an intermediate state of a new kinesin-inhibitor complex. *Biochem. J.* **2010**, *425*, 55–60.
- (46) Dallinger, D.; Kappe, C. O. Rapid preparation of the mitotic kinesin Eg5 inhibitor monastrol using controlled microwave-assisted synthesis. *Nature Protocols* **2007**, *2* (2), 317–321.
- (47) Garcia-Saez, I.; DeBonis, S.; Lopez, R.; Trucco, F.; Rousseau, B.; Thuery, P.; Kozielski, F. Structure of human Eg5 in complex with a

- new monastrol-based inhibitor bound in the R configuration. *J. Biol. Chem.* **2007**, *282* (13), 9740–9747.
- (48) Tarby, C. M.; Kaltenbach, R. F.; Huynh, T.; Pudzianowski, A.; Shen, H.; Ortega-Nanos, M.; Sheriff, S.; Newitt, J. A.; McDonnell, P. A.; Burford, N.; Fairchild, C. R.; Vaccaro, W.; Chen, Z.; Borzilleri, R. M.; Naglich, J.; Lombardo, L. J.; Gottardis, M.; Trainor, G. L.; Roustell, D. L. Inhibitors of human mitotic kinesin Eg5: Characterization of the 4-phenyl-tetrahydrolisoquinoline lead series. *Bioorg. Med. Chem. Lett.* **2006**, *16* (8), 2095–2100.
- (49) Pinkerton, A. B.; Lee, T. T.; Hoffman, T. Z.; Wang, Y.; Kahraman, M. Synthesis and SAR of thiophene containing kinesin spindle protein (KSP) inhibitors. *Bioorg. Med. Chem. Lett.* **2007**, *17* (13), 3562–3569.
- (50) Bohm, H. J. The Computer-Program Ludi - a New Method for the Denovo Design of Enzyme-Inhibitors. *J. Comput.-Aided Mol. Des.* **1992**, *6* (1), 61–78.
- (51) Wolber, G.; Langer, T. LigandScout: 3-d pharmacophores derived from protein-bound Ligands and their use as virtual screening filters. *J. Chem. Inf. Model.* **2005**, *45* (1), 160–169.
- (52) Kirchmair, J.; Distinto, S.; Markt, P.; Schuster, D.; Spitzer, G. M.; Liedl, K. R.; Wolber, G. How to optimize shape-based virtual screening: Choosing the right query and including chemical information. *J. Chem. Inf. Model.* **2009**, *49* (3), 678–692.
- (53) McGaughey, G. B.; Sheridan, R. P.; Bayly, C. I.; Culberson, J. C.; Kreatsoulas, C.; Lindsley, S.; Maiorov, V.; Truchon, J. F.; Cornell, W. D. Comparison of topological, shape, and docking methods in virtual screening. *J. Chem. Inf. Model.* **2007**, *47* (4), 1504–1519.
- (54) Rarey, M.; Kramer, B.; Lengauer, T.; Klebe, G. A fast flexible docking method using an incremental construction algorithm. *J. Mol. Biol.* **1996**, *261* (3), 470–489.
- (55) Linnainmaa, S.; Harwood, D.; Davis, L. S. Pose determination of a 3-dimensional object using triangle pairs. *IEEE Trans. Pattern Anal. Machine Intel.* **1988**, *10* (5), 634–647.
- (56) Lemmen, C.; Lengauer, T. Time-efficient flexible superposition of medium-sized molecules. *J. Comput.-Aided Mol. Des.* **1997**, *11* (4), 357–368.
- (57) Jain, A. N. Surflex: Fully automatic flexible molecular docking using a molecular similarity-based search engine. *J. Med. Chem.* **2003**, *46* (4), 499–511.
- (58) Jones, G.; Willett, P.; Glen, R. C. Molecular recognition of receptor-sites using a genetic algorithm with a description of desolvation. *J. Mol. Biol.* **1995**, *245* (1), 43–53.
- (59) Jones, G.; Willett, P.; Glen, R. C.; Leach, A. R.; Taylor, R. Development and validation of a genetic algorithm for flexible ligand docking. *Abstr. Pap. Am. Chem. Soc.* **1997**, *214*, 154 -COMP..
- (60) Jones, G.; Willett, P.; Glen, R. C.; Leach, A. R.; Taylor, R. Development and validation of a genetic algorithm for flexible docking. *J. Mol. Biol.* **1997**, *267* (3), 727–748.
- (61) Friesner, R. A.; Banks, J. L.; Murphy, R. B.; Halgren, T. A.; Klicic, J. J.; Mainz, D. T.; Repasky, M. P.; Knoll, E. H.; Shelley, M.; Perry, J. K.; Shaw, D. E.; Francis, P.; Shenkin, P. S. Glide: A new approach for rapid, accurate docking and scoring. 1. Method and assessment of docking accuracy. *J. Med. Chem.* **2004**, *47* (7), 1739–1749.
- (62) Venkatachalam, C. M.; Jiang, X.; Oldfield, T.; Waldman, M. LigandFit: a novel method for the shape-directed rapid docking of ligands to protein active sites. *J. Mol. Graph. Model.* **2003**, *21* (4), 289–307.
- (63) Hindle, S. A.; Rarey, M.; Buning, C.; Lengauer, T. Flexible docking under pharmacophore type constraints. *J. Comput.-Aided Mol. Des.* **2002**, *16* (2), 129–149.
- (64) Jorgensen, W. L.; Maxwell, D. S.; TiradoRives, J. Development and testing of the OPLS all-atom force field on conformational energetics and properties of organic liquids. *J. Am. Chem. Soc.* **1996**, *118* (45), 11225–11236.
- (65) Eldridge, M. D.; Murray, C. W.; Auton, T. R.; Paolini, G. V.; Mee, R. P. Empirical scoring functions 0.1. The development of a fast empirical scoring function to estimate the binding affinity of ligands in receptor complexes. *J. Comput.-Aided Mol. Des.* **1997**, *11* (5), 425–445.
- (66) Kiss, R.; Kiss, B.; Konczol, A.; Szalai, F.; Jelinek, I.; Laszlo, V.; Noszal, B.; Falus, A.; Keseru, G. M. Discovery of novel human histamine H4 receptor ligands by large-scale structure-based virtual screening. *J. Med. Chem.* **2008**, *51* (11), 3145–3153.
- (67) de Graaf, C.; Rognan, D. Selective structure-based virtual screening for full and partial agonists of the $\beta 2$ adrenergic receptor. *J. Med. Chem.* **2008**, *51* (16), 4978–4985.
- (68) Evers, A.; Hessler, G.; Matter, H.; Klabunde, T. Virtual screening of biogenic amine-binding G-protein coupled receptors: Comparative evaluation of protein- and ligand-based virtual screening protocols. *J. Med. Chem.* **2005**, *48* (17), 5448–5465.
- (69) Radestock, S.; Weil, T.; Renner, S. Homology model-based virtual screening for GPCR ligands using docking and target-biased scoring. *J. Chem. Inf. Model.* **2008**, *48* (5), 1104–1117.
- (70) Nagarajan, S.; Doddareddy, M. R.; Choo, H.; Cho, Y. S.; Oh, K. S.; Lee, B. H.; Pae, A. N. IKK beta inhibitors identification part I: Homology model assisted structure based virtual screening. *Bioorg. Med. Chem.* **2009**, *17* (7), 2759–2766.
- (71) Liu, T. Q.; Lin, Y. M.; Wen, X.; Jorissen, R. N.; Gilson, M. K. BindingDB: a web-accessible database of experimentally determined protein-ligand binding affinities. *Nucleic Acids Res.* **2007**, *35*, D198–D201.
- (72) Irwin, J. J.; Shoichet, B. K. ZINC - A free database of commercially available compounds for virtual screening. *J. Chem. Inf. Model.* **2005**, *45* (1), 177–182.
- (73) Mosmann, T. Rapid colorimetric assay for cellular growth and survival - application to proliferation and cyto-toxicity assays. *J. Immunol. Methods* **1983**, *65* (1–2), 55–63.